The impact of Last Glacial climate variability in west-European loess revealed by radiocarbon dating of fossil earthworm granules

Olivier Moine[a,1], Pierre Antoine[a], Christine Hatté[b], Amaëlle Landais[b], Jérôme Mathieu[c], Charlotte Prud'homme[a], and Denis-Didier Rousseau[d,e]

[a]Laboratoire de Géographie Physique, Environnements Quaternaires et Actuels, Centre National de la Recherche Scientifique (CNRS)/Université Paris 1 Panthéon-Sorbonne/Université Paris-Est-Créteil-Val-de-Marne (UPEC), 92195 Meudon, France; [b]Laboratoire des Sciences du Climat et de l'Environnement (LSCE)/Institut Pierre-Simon-Laplace, Commissariat à l'Énergie Atomique et aux Énergies Alternatives/CNRS/Université de Versailles-Saint-Quentin-en-Yvelines, Université Paris-Saclay, 91198 Gif-sur-Yvette, France; [c]Sorbonne Universités, Université Pierre-et-Marie-Curie (UPMC)/UPEC/Université Paris-Diderot/CNRS/Institut National de la Recherche Agronomique/Institut de Recherche pour le Développement, Institut d'Ecologie et des Sciences de l'Environnement de Paris, 75005 Paris, France; [d]Laboratoire de Météorologie Dynamique, Ecole Normale Supérieure/CNRS/Ecole Polytechnique/UPMC, Centre de Formation sur l'Environnement et la Société, 75230 Paris, France; and [e]Lamont–Doherty Earth Observatory (LDEO), Columbia University, Palisades, NY 10964-1000

Edited by Edouard Bard, Centre Européen de Recherche et d'Enseignement en Géosciences de l'Environnement, Aix-en-Provence, France, and accepted by Editorial Board Member Thure E. Cerling April 29, 2017 (received for review September 9, 2016)

The characterization of Last Glacial millennial-timescale warming phases, known as interstadials or Dansgaard–Oeschger events, requires precise chronologies for the study of paleoclimate records. On the European continent, such chronologies are only available for several Last Glacial pollen and rare speleothem archives principally located in the Mediterranean domain. Farther north, in continental lowlands, numerous high-resolution records of loess and paleosols sequences show a consistent environmental response to stadial–interstadial cycles. However, the limited precision and accuracy of luminescence dating methods commonly used in loess deposits preclude exact correlations of paleosol horizons with Greenland interstadials. To overcome this problem, a radiocarbon dating protocol has been developed to date earthworm calcite granules from the reference loess sequence of Nussloch (Germany). Its application yields a consistent radiocarbon chronology of all soil horizons formed between 47 and 20 ka and unambiguously shows the correlation of every Greenland interstadial identified in isotope records with specific soil horizons. Furthermore, eight additional minor soil horizons dated between 27.5 and 21 ka only correlate with minor decreases in Greenland dust records. This dating strategy reveals the high sensitivity of loess paleoenvironments to Northern Hemisphere climate changes. A connection between loess sedimentation rate, Fennoscandian ice sheet dynamics, and sea level changes is proposed. The chronological improvements enabled by the radiocarbon "earthworm clock" thus strongly enhance our understanding of loess records to a better perception of the impact of Last Glacial climate changes on European paleoenvironments.

millennial-timescale climate change | radiocarbon dating | earthworm calcite granules | Last Glacial loess | Europe

Millennial-timescale alternations of Greenland stadials (GSs) and Greenland interstadials (GIs) forming Dansgaard–Oeschger cycles are global climate changes well-expressed in Last Glacial ice cores (1) and marine sediment proxy records (2), but their causes and mechanisms are still debated (3–5). Modeling results show that the European climate was particularly impacted by switches between weakened or enhanced modes of the Atlantic Meridional Overturning Circulation through the transportation of North Atlantic air masses by Westerlies (6). Still, there are growing evidences that Greenland high-resolution climate records do not exhibit the full lower-latitude climate variability, especially during cold periods (i.e., no distinction of Heinrich events) (7, 8). There is thus an urgent need for well-dated high-resolution records of millennial-timescale climatic variability at midlatitudes. Although many speleothems, marine, and lake sediment records are available in the Mediterranean domain (9–11), continental regions of Northern Europe are not adequately documented, and very few radiometric ages are available for records north of 45° N. However, aeolian periglacial deposits forming the European Loess Belt (Fig. 1) are the most widespread sedimentary archive available for the detailed study of Last Glacial climatic and environmental changes in continental Europe (12).

The best loess sequences, owing to their high sedimentation rate that can reach 0.5–2 m/ka during the 35- to 17-ka time interval (13, 14), are indeed well-suited to study millennial-timescale environmental changes. High-resolution stratigraphy, paleopedology, grain size, magnetic properties, malacology, and organic and isotopic geochemistry can be used to reconstruct rapid variations of aeolian dynamics, relative temperatures, paleoprecipitation, and vegetation cover during the Last Glacial (15). During the Middle and Upper Pleniglacial [i.e., roughly marine isotope stage 3 (MIS 3) and MIS 2], the cyclical alternation of loess units with 0.3- to 0.5-m-thick tundra gley horizons (i.e., gelic gleysols resulting from the seasonal thaw of a permafrost active layer in tundra environments) or arctic to boreal brown soils (i.e., cambisols characterized by a slight weathering of the parent material in shrub-tundra environments) suggests a close connection with the succession of GS and GI identified in other archives. This link is supported by the strong relationship

Significance

Last Glacial millennial-timescale warming phases well-recorded in Greenland ice cores are relevant across the Northern Hemisphere. However, dating limitations in loess deposits inhibited characterizing their impact on the European Great Plain. Here, the radiocarbon dating of a large set of earthworm calcite granule samples from the Nussloch reference loess sequence (Rhine Valley, Germany) led to a straightforward chronological distinction of all soil horizons. Resulting correlations with Greenland interstadials between 50 and 20 ka also revealed more complex climate dynamics than interpreted from Greenland $\delta^{18}O$ records. This study is a fundamental contribution to understanding links between mid- and high-latitude climate changes and their spatial and temporal impact on paleoenvironments and prehistoric population settlement in Europe.

Author contributions: O.M. and P.A. designed research; C.H. and J.M. contributed new reagents/analytic tools; O.M., P.A., and A.L. analyzed data; and O.M., P.A., C.H., A.L., J.M., C.P., and D.-D.R. wrote the paper.

The authors declare no conflict of interest.

This article is a PNAS Direct Submission. E.B. is a guest editor invited by the Editorial Board.

[1]To whom correspondence should be addressed. Email: olivier.moine@lgp.cnrs.fr.

This article contains supporting information online at www.pnas.org/lookup/suppl/doi:10.1073/pnas.1614751114/-/DCSupplemental.

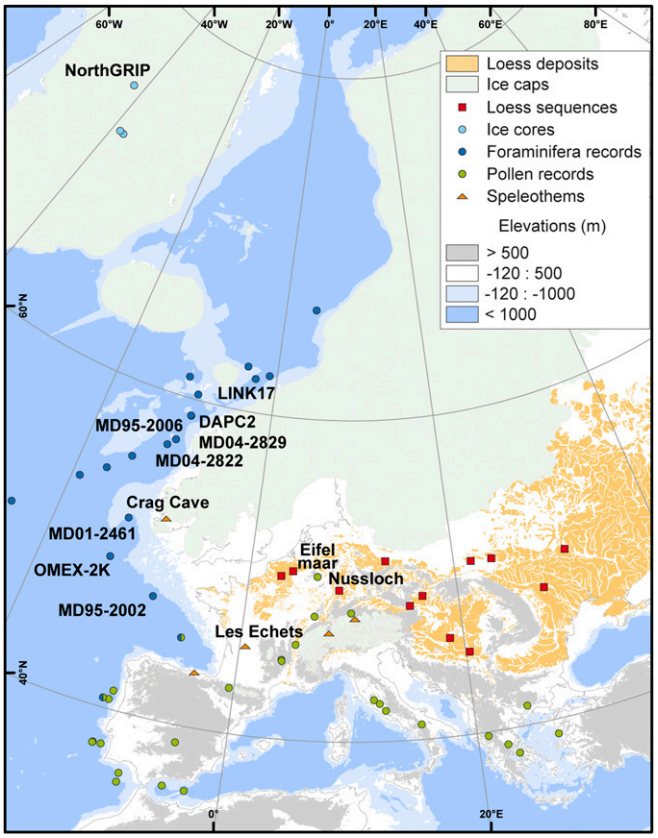

Fig. 1. Location of the Nussloch site in the European Loess Belt. Last Glacial records discussed in the text are named.

between the types of paleosols in the loess records and both duration and intensity of associated GI (16). However, limitations in absolute dating of loess sequences still inhibit the use of this type of terrestrial record for depicting regional climatic and environmental changes in association with GI. Archaeological layers aside, the scarcity of organic remains, such as wood, charcoal, and bone, results in a lack of reliable radiocarbon ages. Optically stimulated luminescence (OSL) methods ubiquitously used in loess do not solve this problem owing to their inherent 10% error margins. Poor chronological control weakens our proposed correlations and conceptual model linking loess–tundra gley alternations with GS–GI cycles (14, 17), which are based on (*i*) the succession pattern of both soil horizons and GI, (*ii*) the relative importance of the different events in both records, and (*iii*) correspondences between major variations of two Aeolian dynamic proxies [i.e., the loess grain size index and the Greenland ice core dust (Ca^{2+}) concentration] (18). Despite its coherency, this correlation scheme remains partially debated (19) and still requires validation by a precise and accurate independent chronology.

Results

Here, we present a consistent radiocarbon chronology of all Middle and Upper Pleniglacial paleosols of the Nussloch loess sequence from a promising radiocarbon dating methodology applied to earthworm calcite granules (Fig. 2), hereafter simply referred to as granules (*Methods*). Granules are scarce in loess units but very abundant in tundra gleys and arctic to boreal brown soils (20). Many factors render granules interesting and optimum for precise chronology: (*i*) granule carbon is mainly derived from feeding sources (i.e., litter), (*ii*) experiments on *Lumbricus terrestris* revealed a very low content in old or dead carbon from soils in granule $\delta^{13}C$ (21), (*iii*) granules are mainly released at the soil surface (22), (*iv*) evidence of earthworm-induced bioturbation is absent in tundra gleys and very rare in arctic to boreal brown soils according to both field and thin-section observations, and (*v*) the earthworm habitat is restricted to a depth of a few decimeters between the surface and the permafrost table in tundra gley horizons given the periglacial conditions essential to their formation, which is not necessarily the case in arctic to boreal brown soils that did not develop on permafrost. Taking into account all of these specificities, risks of age overestimation resulting from old carbon pollution and age underestimation caused by artificial time shifts between granules and sediment are strongly limited (more details are in *Methods*). The Nussloch site shows the most complete pedostratigraphic succession of Western Europe between 55 and 20 ka (14, 23) (Fig. S1). It is thus ideal for this application of granule radiocarbon dating in a loess context. We constructed a composite record including all pedostratigraphic units by stacking the upper 11.5 m of P4 profile on the lower 7 m of P8 profile (Fig. S2). All ages of soil horizons from P3, P4, and P8 profiles (Table S1) were then transposed onto the composite record (Fig. 3 and Fig. S2).

Calibrated ages range between 44,949–48,595 and 13,814–14,453 ka cal. B.P. (Table S1). Most of the 2σ errors are of 0.6–2.5% (100–800 y) from 36 to 13 ka cal. B.P. and 1.9–3.7% (700–1,500 y) from 44 to 38 ka cal. B.P. and vary more largely between 3.9% (1,800 y) and 7.0% (3,300 y) approaching the age limit of radiocarbon dating. However, these uncertainties are significantly lower than those of luminescence ages and similar to those of the latest Greenland age model ranging from ∼0.17 to ∼2.3 ka for this time interval (24). Only two ages seem largely underestimated: the age from incipient gley 8b (IG8b) on P8 by 3.5 ka compared with its equivalent on P4, and the age from IG9b on P4 by 7 ka compared with that extrapolated from the sedimentation rate (Fig. 3 and Table S1). In their respective profiles, both are located about 1.5 m below the present day surface within a zone bioturbated by modern roots and earthworms (Fig. S1). We consider that these two samples are probably contaminated by postglacial to modern granules. With

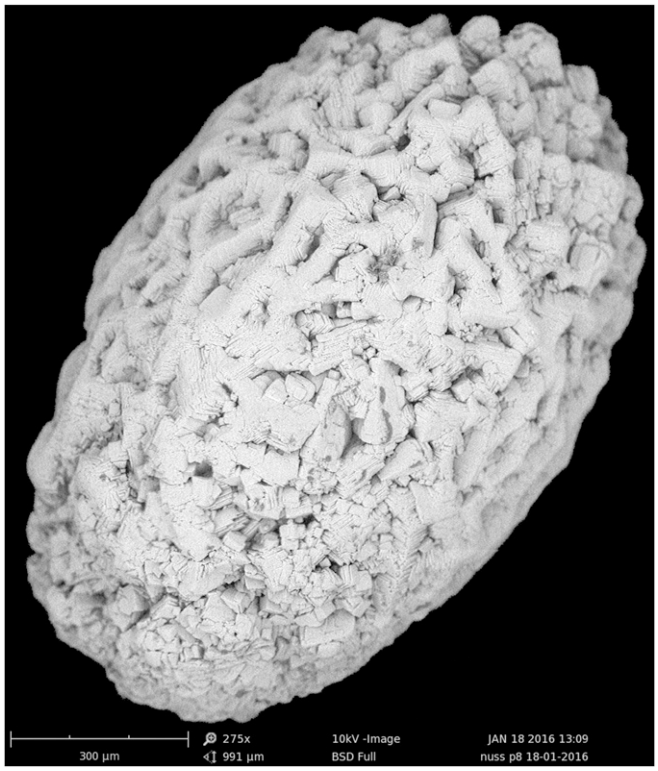

Fig. 2. Scanning electron microscope (SEM) view of a fossil carbonate granule of *Lumbricus* earthworm from the Nussloch P8 loess profile. BSD, backscattered electron detector. Modified from CoDEM/BATLAB.

the above two results discarded, all remaining ages define a chronological series with no statistically significant age inversion. Age reproducibility checks performed in tundra gley units Gm3 and G1a on P8 are positive (Fig. 3 and Table S1). Ages from arctic to boreal brown soils fit well among tundra gleys ages. Ages from tundra gleys Gm3 and Gm1, located only 40 cm below the base of the Lohne Soil and the Upper Gräselberg Soil, respectively, do not seem rejuvenated as one might expect if bioturbation related to these more developed soils was important (Table S1). In absence of deep earthworm activity in these permafrost-free paleosols, dated granules might have mainly been produced by epigeic earthworms living close to the soil surface rather than anecic earthworms that usually dig deep burrows (25). Reliable ages are thus obtained from all tundra gleys and arctic to boreal brown soils as long as they are not affected by deep bioturbations from the topsoil. The regular distribution of radiocarbon ages throughout the loess profile indicates an almost continuous sedimentation between 50 and 20 ka. Sedimentation rates derived for the 45- to 21-ka interval are higher in loess units than in pedogenetic horizons. They increase from 0.19 mm/y for the Middle Pleniglacial to 0.33 and 1.12 mm/y for the early and full Upper Pleniglacial, respectively (Fig. 3), matching previous estimates based on luminescence ages and previous correlations with Greenland (14). We can now confidently establish correlations with other archives over the entire Nussloch sequence and especially after 30 ka.

Discussion

Two major changes in sedimentary and environmental dynamics are evidenced in the Nussloch loess sequence records. The first one around 30 ka presents a major limit marked by a sharp and strong increase in both sedimentation rate (Fig. 3) and grain size index (GSI) (14). These features observed in almost all of the loess sequences from Western to Eastern Europe (26–30) thus constitute a major marker level for stratigraphic correlations. This marker level at ∼30 ka is, within limit uncertainties, synchronous with (*i*) a first step of expansion of the Last Glacial maximum (LGM) Fennoscandian ice sheet and mountain ice caps because of higher precipitations (31, 32), (*ii*) a significant drop in sea level from about −60 to −100 m (33), and (*iii*) a change from anastomosing to higher-energy braided channels in west European fluvial systems (34). This configuration induced a widening of deflation areas on the continental shelves of the North Sea and Channel and in large river valleys and a very strong increase in detrital particles available for Aeolian deflation and transport, enabling the deposition of markedly thicker loess units over Europe (35). A second marker level, observed around 23 ka at the top of tundra gley G7, is characterized by a sharp decrease in the GSI, an almost complete disappearance of the rich mollusk fauna of Nussloch (17), a shift from finely laminated to homogeneous loess in Western and Central Europe (26, 27, 30), and a significant increase in the sand content in Eastern Europe (28, 29). This marker level at ∼23 ka, also recorded across the European Loess Belt, indicates a shift to markedly more arid conditions between 23 and 20 ka contemporaneous with maxima in ice sheet extension and volume. However, very low sea level and high-energy braided channels in the deflation areas persisted during this time interval, permitting high loess sedimentation rate (∼1 mm/y) to be maintained in European loess profiles.

Furthermore, based on our radiocarbon chronology, reliable correlations between the pedostratigraphical sequence of Nussloch and Greenland climate proxy records over the 55- to 20-ka interval can now be established (Fig. 3). Each tundra gley and arctic to boreal brown soils correlates with a single GI within dating uncertainties (*Methods*). The only two exceptions are related to low sedimentation rates during the Middle Pleniglacial. The tundra gley Gm3, which is twice the thickness of Gm2 and Gm1, most likely stacks two successive tundra gleys formed during GI 11 and GI 10 (i.e., during the Hengelo interstadial) (36, 37). Similarly, the Lohne Soil appears likely as a stack of two soil horizons developed during GI 8 and GI 7c (i.e., during the initial phase of the Denekamp interstadial complex) (36). Our chronology thus confirms and updates previous correlations (Table S2) based on Aeolian dynamic proxies. Around 50° N, Crag Cave speleothems (southwest Ireland) constitute the only other record of most Last Glacial interstadials. Indeed, their growth phases are induced by climate ameliorations contemporaneous to GI (38) as well as mollusk abundance increases in Nussloch soil horizons (17, 39). However, speleothem growth ceases during stadials, whereas loess deposition continues, hence revealing additional variability.

We can thus distinguish, within Nussloch loess units above tundra gley G4, eight additional slightly hydromorphic horizons with oxidized root tracks, hereafter called IGs, dated between about 27 and 21 ka (Fig. 3). By comparison with tundra gleys, IGs are thinner (only 10- to 15-cm thick) and have weaker iron redox imprints, implying a thinner permafrost active layer with lower ice content and weaker water release during the thawing season. Changes in mollusk assemblages recorded in IGs from Nussloch profile P3 also reflect weaker humidity increases as well as weaker or similar decreases in vegetation diversity but no appreciable warming phase (17) compared with tundra gleys. Likewise, magnetic properties of the sediment studied at high resolution throughout Nussloch profile P8 led to a similar conclusion (40). Although Nussloch tundra gleys are always associated with strong decreases in GSI and Greenland $[Ca^{2+}]$ (14), it is not systematic for IGs (Fig. 4). Moreover, no significant $\delta^{18}O$ increases in Greenland records can be identified in contemporaneous time intervals to IGs. The formation of these IGs may thus imply weaker precipitation increases and northward shifts of the Polar front than those leading to the formation of the main tundra gleys. The radiocarbon chronology established from the Nussloch loess sequence thus reveals a more complex pattern than identified until now within MIS 2 in Greenland $\delta^{18}O$ records. Indeed, the unsuspected centennial environmental variability exhibited in the Nussloch loess record during MIS 2 shows that the LGM was probably not as stable as generally admitted.

Among records that display short and low-magnitude oscillations during MIS 2, one can cite for the North Atlantic Ocean those of *Neogloboquadrina pachyderma* (sinistral) percentages from the Rockall Trough (41, 42) (Fig. 1), the Cariaco Basin reflectance influenced by movements of the Intertropical Convergence Zone (43), and the Bermuda Rise calcium concentration influenced by the Atlantic Meridional Overturning Circulation (44) (Fig. 4). In Europe, both Les Echets Lake magnetic susceptibility (45) and Eifel maar varve thickness (46) were likely influenced by the Aeolian transport, and in China, the Qinghai Lake dust flux above 25 μm was influenced by the Westerlies (47). The acquisition of more high-resolution and well-dated terrestrial and marine records is thus required to thoroughly evaluate the significance of both IGs and minor LGM oscillations. Additional development of coupled modeling experiments will be necessary to improve our understanding of associated climate mechanisms and interactions.

Future applications of this radiocarbon dating strategy based on earthworm calcite granules will improve correlations between loess sequences. This fundamental step forward will contribute to build a well-dated reference environmental framework across the European Loess Belt for the study of late Neanderthal and early Anatomically Modern Human peopling of Europe and their interactions with climate and environmental changes.

Methods

The Choice of Earthworm Calcite Granules for Radiocarbon Dating. West European Last Glacial loess sequences generally lack organic remains, such as wood, charcoals, and bones, which are required for radiocarbon dating. In this area, only particular geomorphological structures, like the Nussloch thermokarst infillings (19, 23) (Fig. S1 and Table S1), or archeological levels, may provide these materials that only exceptionally yield long-term coherent chronologies as, for example, in Central Europe (48, 49). A ubiquitous carbon-bearing material should thus be identified. To address the issue of a detailed chronology for the Last Glacial, the dating of loess bulk organic matter has been used throughout the Nussloch loess sequence (50). Despite a better precision than for OSL ages, these results show age underestimations

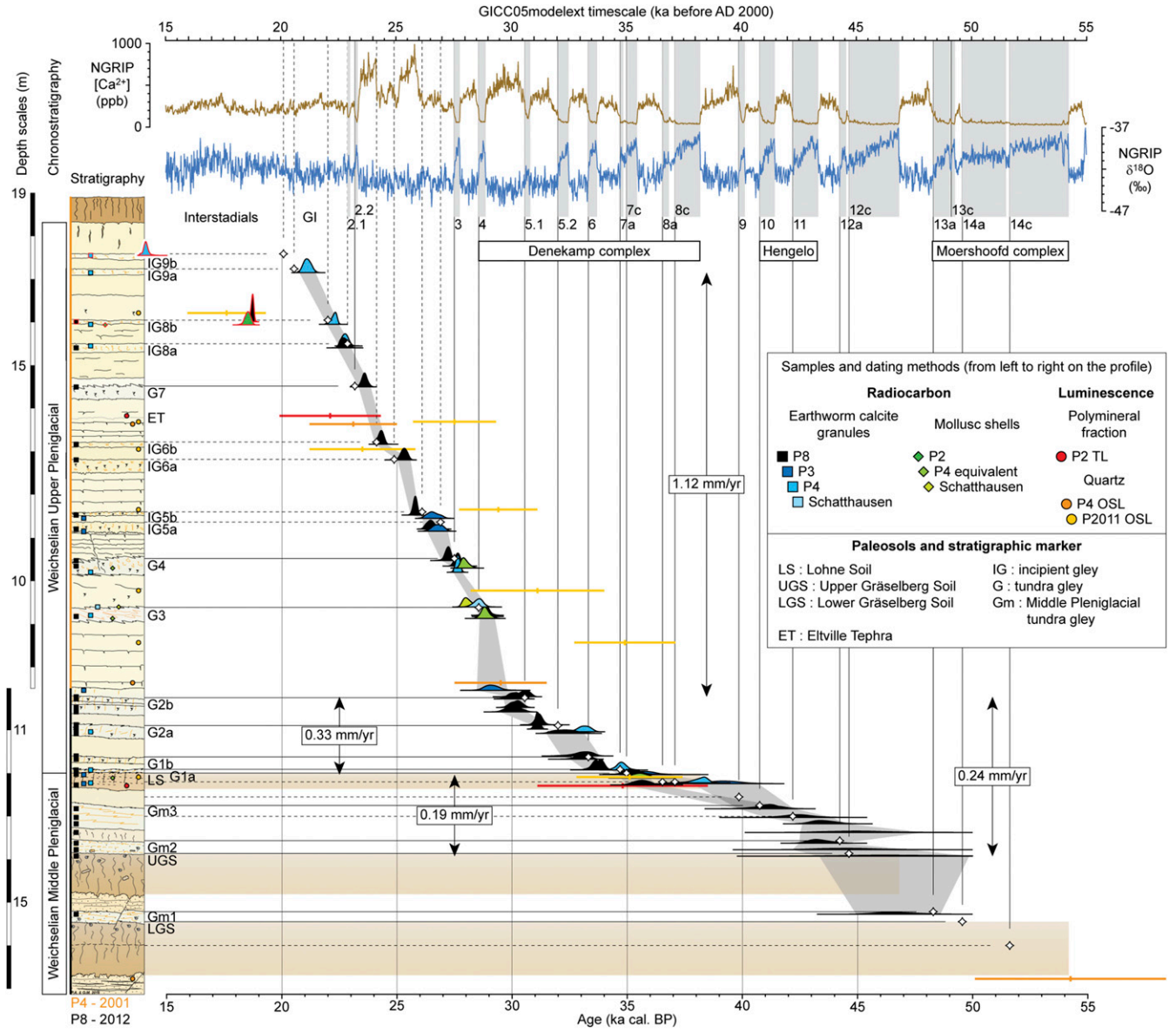

Fig. 3. Radiocarbon chronology of all soil horizons from the Nussloch P4–P8 composite loess profile based on earthworm granules and correlations with GIs. Discarded ages are red-contoured. The gray shading indicates 2σ ranges of ^{14}C ages. Dashed lines highlight IGs and contemporaneous minor decreases in Greenland $[Ca^{2+}]$ records (24). Table S1 shows values and references of all displayed ages. TL, thermoluminescence.

and inversions, especially for tundra gley horizons (51). In addition, radiocarbon ages are, like feldspar OSL ages (14, 52, 53), significantly younger than quartz OSL and thermoluminescence ages (54–56). Alternatively, radiocarbon dating of terrestrial mollusk shells has been occasionally attempted from loess deposits (57–59). However, their results have always been criticized because of the possible incorporation of an undetermined fraction of old carbon in the shells (60). Despite this problem and the possible pollution by modern carbonates that could alter age accuracy, promising results have recently been obtained from several minute taxa from North American Quaternary deposits (61) and for the Nussloch P4 section (Germany) (53). In contrast, the few dates obtained from calcified root cells indicated that their formation can be significantly younger than the deposition of the surrounding sediment (62).

These results led us to look for another ^{14}C dating support for loess sequences. In this context, we noted the presence of numerous small calcite granules in the sieving residues resulting from the malacological study of the Nussloch P3 profile, especially in tundra gley horizons and arctic to boreal brown soils. It was then decided to test their chronological potential.

Characteristics of Earthworm Calcite Granules. Earthworm calcite granules generally have an ovoid form, ranging in size from 0.01 to 2.5 mm and, are composed of aggregated sparite crystals organized in a radial structure achieved before their excretion (63) (Fig. 2). They are produced in Morren's glands that are laterally connected to the earthworm esophagus. Fixed by enzymatic reactions in these glands (64), calcium carbonate carbon originates mostly from feeding, essentially from litter and very few from humus and breathed atmospheric CO_2 (21). In addition, contributions in old and dead mineral carbon from soils are also extremely weak by *L. terrestris* (21), which limits any eventual artificial aging of dated granules.

Autopsies and breeding experiments revealed that earthworms of the genus *Lumbricus* are the largest granule producers among the most common European taxa. Selecting granules larger than 0.5 mm (22), which only *Lumbricus* taxa are able to produce, restrains any variability that could result from a multigenus material. Moreover, because the quantity of granules produced by *Lumbricus* species and excreted in the litter exceeds by one to two orders of magnitude the quantity excreted in the top 10 cm of the soil (22), they are then contemporaneous from the vegetation growing on the surface of the soil in which earthworms lived.

High-resolution counts recently undertaken throughout French Upper Weichselian loess sequences revealed very high *Lumbricus* granule abundances in tundra gley horizons and arctic brown soils (several hundred per 10 L of

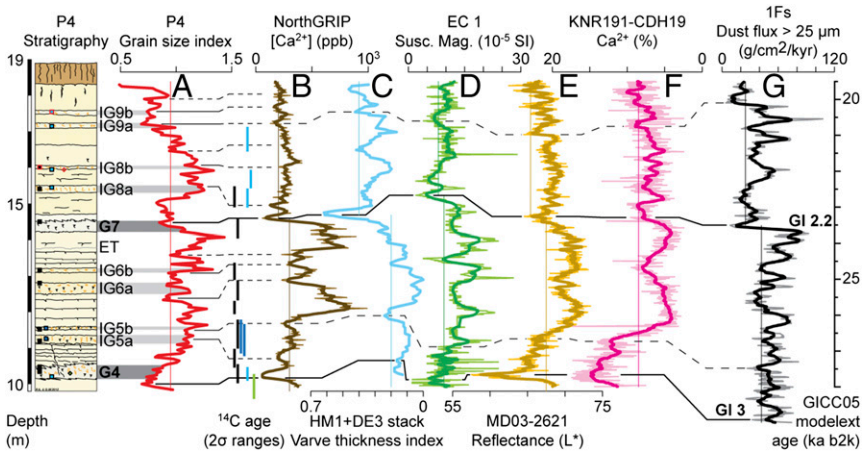

Fig. 4. Correlation attempt of Nussloch pedostratigraphy and GSI record with several different Northern Hemisphere paleoclimate records from 28 to 19.5 ka b2k (before AD 2000). (*A*) Nussloch P4 (14); (*B*) NorthGRIP (24) plus 5 samples moving average signals; (*C*) Eifel maar (46); (*D–F*) Les Echets Lake (45), Cariaco Basin (43), and Bermuda Rise (44) plus 21 samples moving average signals; and (*G*) Qinghai Lake (47) plus 11 samples moving average signals. Solid lines highlight established correlations between tundra gleys and interstadials. Short dashed lines highlight tentative correlations between Nussloch and other record.

sediment) and very low to zero abundances in loess units (20). Abrupt shifts in granule concentration associated with these stratigraphic transitions confirm their very low vertical dispersion. Moreover, in Last Glacial tundra gley horizons, which correspond to past permafrost active layers, earthworms were confined to the 0.2- to 0.4-m uppermost part of the soil profile that was unfrozen during the warm season. This restriction of their distribution prevented the creatures from any ingestion of old carbon from frozen underlying deposits. In addition, the absence of earthworm galleries and hibernation chambers in both tundra gleys and arctic brown soils suggests a strongly reduced burrowing activity in these layers, resulting from both superficial distribution during the warm season and feeding strategy in litter of *Lumbricus* species during milder and more humid seasons, like spring and autumn (25). The very low organic carbon content in loess (~0.1% wt), as in boreal and arctic brown soils (~0.4% wt), also strongly limits all eventual contribution of old or dead carbon in granules. Finally, the scarcity or absence of granules in pure loess units precludes any pollution of immediately underlying tundra gleys by younger fossil granules. In tundra gleys and arctic brown soils, high concentration in granules also allows for the sampling of thin sediment slices down to only 5-cm thick and including up to several hundred granules.

All of these criteria, therefore, favor the determination of accurate and precise ^{14}C ages from granules. However, the few trials of ^{14}C dating of granules (57, 62, 65, 66) remained insufficient to show their reliability in loess contexts. To provide a reliable chronology of continental interstadials, we decided to focus on the Nussloch loess–paleosol sequence that presents the best stratigraphic resolution for the Last Glacial in Western Europe (14, 23) (*SI Text*).

Acquisition of Modern and Fossil Earthworm Calcite Granules. In vitro breeding experiments have been conducted for 1 mo under controlled temperature (12-h diurnal cycle fluctuating between 14 °C and 16 °C with light) in plastic containers filled in with granule-free breeding ground; 20 g of calcium carbonate has been added to one of the containers. At the end of the experiments, granules have been collected from the uppermost 1–2 cm of experimental soil.

Fossil granules have been extracted from mollusk samples sieving residues from Nussloch P3, P4, and P8 profiles located along the axis of the same loess dune or "greda" (14, 23). Samples for terrestrial mollusks are systematically 10-L large, but those of the P8 profile were 5-cm thick and therefore, twice as thin as those of P3 and P4 profiles. All modern and fossil samples have been wet sieved on a 425-µm mesh.

Breeding experiments led on eight common European taxa revealed that only species from the *Lumbricus* genus are able to produce granules larger than 0.5 mm (22). Owing to the large granule abundance in selected samples, the use of a 0.8-mm mesh was sufficient to collect enough material for dating purpose. All granules have been hand-picked under binocular microscope with an initial optical selection of the cleanest ones and then washed for 10 min in distilled water in an ultrasonic tank to remove all eventual surface pollution (clay, iron oxides, and organomineral coatings). After drying, we selected under binocular 50 granules among the largest and visually cleanest to reach a minimum mass of 50 mg for each sample.

Radiocarbon Dating Protocol of Earthworm Calcite Granules. Granules were then slightly crushed in an agate mortar. All samples were leached with 0.01 M HNO_3 at room temperature for at least 30 min and rinsed with Milli-Q water to remove superficial contamination and oxidize any remaining organic matter. Extra water is removed using a Pasteur pipette.

At Laboratoire de Mesure du Carbone 14, samples were introduced into the bottom of a two-fingers reactor (67) and 1 cm^3 of pure H_3PO_4 (100%; previously distilled for 3 d at 105 °C and stored under argon) is added into the lateral reservoir. The reactor with the wet sample and H_3PO_4 is rapidly connected to the semiautomated vacuum line. The sample is then dried on the line, and the reactor is manually rotated to pour H_3PO_4 onto the samples (67).

At the Poznan Radiocarbon Laboratory, samples are introduced into a vial and dried under vacuum. Argon is introduced into the vial (up to overpressure). Vial is opened for a while just to introduce H_3PO_4 into the side arm of it. Argon is pumped out, and H_3PO_4 is poured onto the sample just afterward. Subsequent steps are similar in both laboratories: CO_2 evolving, water elimination, and evaluation of C quantity. CO_2 reduction and ^{14}C activity measurements are performed in Saclay (67, 68) and Poznan (69, 70) according to their respective protocols and equipment.

Check of Method Reliability. Radiocarbon dating of granules produced in laboratory breeding with and without addition of calcium carbonate yielded modern ages [101.8 ± 0.3 and 101.7 ± 0.4 pMC (percent modern carbon), respectively]. Thus, despite an age of 48,330 ± 2,370 B.P. (i.e., 0.24 ± 0.07 pMC) for the added calcium carbonate, both granule samples yielded ages similar to that of the soil organic matter from the breeding (270 ± 30 B.P.; i.e., 96.0 ± 0.3 pMC). Contribution in dead carbon of soil carbonates is undetectable and thus, negligible as previously concluded from isotope studies (21).

Probability distributions of calibrated granule-based radiocarbon ages have been generated using CALIB 7.0.2. software based on the IntCal13 calibration curve (71).

Comparisons of Nussloch and Greenland Chronologies. Because pedostratigraphic units result from a variable combination of weathering (downward) and Aeolian sedimentation (upward) processes, linking their lower and upper limits with onsets and offsets of GI is still not straightforward. The 2σ ranges of 35 calibrated ^{14}C ages from the main soil horizons have thus been compared with time intervals of the correlated GI. The maximum counting errors (MCEs) of the GICC05modelext age model (24), regarded as 2σ uncertainties, provide uncertainties on GI onsets and offsets. Extended GI time intervals at 1σ and 2σ have thus been calculated with one-half and full MCE values, respectively. All ^{14}C ages present an overlap with their associated GI 2σ intervals, and two ages from tundra gley G1a and G2a miss the overlap with GI 1σ intervals by only 87 and 134 y, respectively (Fig. S3). Most of ^{14}C ages present an overlap of 100% with GI 2σ intervals and above 60% for others. Also, 75% of the ^{14}C ages present an overlap higher than 50% with GI 1σ intervals, and for 90% of them, the overlap is higher than 35%. The distributions of these overlap values vs. the median value of the calibrated ^{14}C age show no particular trend.

ACKNOWLEDGMENTS. We thank Dr. Manfred Löscher for his logistical help and during fieldwork and sampling campaigns; Prof. Zhisheng An for original data on Qinghai Lake; Prof. Philip Gibbard and Dr. France Lagroix for their comments about the manuscript and editorial help; Ingrid Caffy from Laboratoire de Mesure du Carbone 14 (LMC14), who checked the reliability and appropriateness of the proposed protocol on preliminary samples; Dr. Daniel Brunstein for geographical information system mapping of Fig. 1; the three anonymous reviewers for their constructive remarks; the Heidelberg Cement Company for allowing the fieldwork in the Nussloch quarry; both the Poznan Radiocarbon Laboratory and the LMC14 laboratory that underwent ^{14}C dating; and the CoDEM/BATLAB for the

SEM photographs of earthworm calcite granule. This study was supported by Grant ANR-08-BLAN-0227 from Agence Nationale de la Recherche (to D.-D.R., P.A., C.H. and O.M.), by a project from CNRS "Projets Exploratoires Premier Soutien" program (to P.A. and O.M.), and by CNRS ARTEMIS calls for ^{14}C dating (to O.M., P.A. and C.H.). This paper is LDEO contribution no. 8109 and LSCE contribution no. 6161.

1. Dansgaard W, et al. (1993) Evidence for general instability of past climate from a 250-kyr ice-core record. *Nature* 364:218–220.
2. Sánchez Goñi MF, Harrison SP (2010) Millennial-scale climate variability and vegetation changes during the Last Glacial: Concepts and terminology. *Quat Sci Rev* 29:2823–2827.
3. Rasmussen TL, Thomsen E, Moros M (2016) North Atlantic warming during Dansgaard-Oeschger events synchronous with Antarctic warming and out-of-phase with Greenland climate. *Sci Rep* 6:20535.
4. Baldini JUL, Brown RJ, McElwaine JN (2015) Was millennial scale climate change during the Last Glacial triggered by explosive volcanism? *Sci Rep* 5:17442.
5. Zhang X, Lohmann G, Knorr G, Purcell C (2014) Abrupt glacial climate shifts controlled by ice sheet changes. *Nature* 512:290–294.
6. Flückiger J, Knutti R, White JWC, Renssen H (2008) Modeled seasonality of glacial abrupt climate events. *Clim Dyn* 31:633–645.
7. Rhodes RH, et al. (2015) Paleoclimate. Enhanced tropical methane production in response to iceberg discharge in the North Atlantic. *Science* 348:1016–1019.
8. Guillevic M, et al. (2014) Evidence for a three-phase sequence during Heinrich Stadial 4 using a multiproxy approach based on Greenland ice core records. *Clim Past* 10:2115–2133.
9. Fletcher WJ, et al. (2010) Millennial-scale variability during the last glacial in vegetation records from Europe. *Quat Sci Rev* 29:2839–2864.
10. Luetscher M, et al. (2015) North Atlantic storm track changes during the Last Glacial Maximum recorded by Alpine speleothems. *Nat Commun* 6:6344.
11. Moreno A, et al. (2014) A compilation of Western European terrestrial records 60–8 ka BP: Towards an understanding of latitudinal climatic gradients. *Quat Sci Rev* 106:167–185.
12. Haase D, et al. (2007) Loess in Europe—its spatial distribution based on a European Loess Map, scale 1:2,500,000. *Quat Sci Rev* 26:1301–1312.
13. Frechen M, Oches EA, Kohfeld KE (2003) Loess in Europe—mass accumulation rates during the Last Glacial period. *Quat Sci Rev* 22:1835–1857.
14. Antoine P, et al. (2009) Rapid and cyclic aeolian deposition during the Last Glacial in European loess: A high-resolution record from Nussloch, Germany. *Quat Sci Rev* 28:2955–2973.
15. Rousseau D-D, Derbyshire E, Antoine P, Hatté C (2007) Loess records. Europe. *Encyclopedia of Quaternary Science*, ed Elias SA (Elsevier, Amsterdam), pp 1440–1456.
16. Rousseau D-D, et al. (2007) Link between European and North Atlantic abrupt climate changes over the last glaciation. *Geophys Res Lett* 34:L22713.
17. Moine O, Rousseau D-D, Antoine P (2008) The impact of Dansgaard-Oeschger cycles on the loessic environment and malacofauna of Nussloch (Germany) during the Upper Weichselian. *Quat Res* 70:91–104.
18. Rousseau D-D, et al. (2002) Abrupt millennial climatic changes from Nussloch (Germany) Upper Weichselian eolian records during the Last Glaciation. *Quat Sci Rev* 21:1577–1582.
19. Kadereit A, Kind C-J, Wagner GA (2013) The chronological position of the Lohne Soil in the Nussloch loess section – re-evaluation for a European loess-marker horizon. *Quat Sci Rev* 59:67–86.
20. Prud'homme C, et al. (2015) Earthworm calcite granules: A new tracker of millennial-timescale environmental changes in Last Glacial loess deposits. *J Quat Sci* 30:529–536.
21. Canti MG (2009) Experiments on the origin of ^{13}C in the calcium carbonate granules produced by the earthworm *Lumbricus terrestris*. *Soil Biol Biochem* 41:2588–2592.
22. Canti M, Piearce TG (2003) Morphology and dynamics of calcium carbonate granules produced by different earthworm species. *Pedobiologia (Jena)* 47:511–521.
23. Antoine P, et al. (2001) High-resolution record of the last Interglacial-glacial cycle in the Nussloch loess-paleosol sequences, Upper Rhine Area, Germany. *Quat Int* 76-77:211–229.
24. Rasmussen SO, et al. (2014) A stratigraphic framework for abrupt climatic changes during the Last Glacial period based on three synchronized Greenland ice-core records: Refining and extending the INTIMATE event stratigraphy. *Quat Sci Rev* 106:14–28.
25. Rundgren S (1975) Vertical distribution of lumbricids in southern Sweden. *Oikos* 26:299–306.
26. Antoine P, et al. (2013) High-resolution record of the environmental response to climatic variations during the Last Interglacial–Glacial cycle in Central Europe: The loess-palaeosol sequence of Dolní Věstonice (Czech Republic). *Quat Sci Rev* 67:17–38.
27. Antoine P, et al. (2016) Upper Pleistocene loess-palaeosol records from Northern France in the European context: Environmental background and dating of the Middle Palaeolithic. *Quat Int* 411:4–24.
28. Haesaerts P, et al. (2003) The East Carpathian loess record: A reference for the Middle and Late Pleniglacial stratigraphy in Central Europe. *Quaternaire* 14:163–188.
29. Rousseau D-D, et al. (2011) North Atlantic abrupt climatic events of the last glacial period recorded in Ukrainian loess deposits. *Clim Past* 7:221–234.
30. Meszner S, Kreutzer S, Fuchs M, Faust D (2013) Late Pleistocene landscape dynamics in Saxony, Germany: Paleoenvironmental reconstruction using loess-paleosol sequences. *Quat Int* 296:97–104.
31. Hughes AC, et al. (2016) The last Eurasian ice sheets – a chronological database and time-slice reconstruction, DATED-1. *Boreas* 45:1–45.
32. Ivy-Ochs S, et al. (2008) Chronology of the last glacial cycle in the European Alps. *J Quat Sci* 23:559–573.
33. Clark PU, et al. (2009) The last glacial maximum. *Science* 325:710–714.
34. Vandenberghe J (2003) Climate forcing of fluvial system development: An evolution of ideas. *Quat Sci Rev* 22:2053–2060.
35. Sima A, et al. (2009) Imprint of North-Atlantic abrupt climate changes on western European loess deposits as viewed in a dust emission model. *Quat Sci Rev* 28:2851–2866.
36. Puzachenko AY, et al. (2016) The Eurasian mammoth distribution during the second half of the Late Pleistocene and the Holocene: Regional aspects. *Quat Int*, 10.1016/j.quaint.2016.05.019.
37. Vandenberghe J, van der Plicht J (2016) The age of the Hengelo interstadial revisited. *Quat Geochronol* 32:21–28.
38. Fankhauser A, McDermott F, Fleitmann D (2016) Episodic speleothem deposition tracks the terrestrial impact of millennial-scale last glacial climate variability in SW Ireland. *Quat Sci Rev* 152:104–117.
39. Moine O, Rousseau D-D, Antoine P (2005) Terrestrial molluscan records of Weichselian Lower to Middle Pleniglacial climatic changes from the Nussloch loess series (Rhine Valley, Germany): The impact of local factors. *Boreas* 34:363–380.
40. Taylor SN, Lagroix F (2015) Magnetic anisotropy reveals the depositional and post-depositional history of a loess-paleosol sequence at Nussloch (Germany). *J Geophys Res Solid Earth* 120:2859–2876.
41. Austin WEN, et al. (2012) The synchronization of palaeoclimatic events in the North Atlantic region during Greenland Stadial 3 (ca 27.5 to 23.3 kyr b2k). *Quat Sci Rev* 36:154–163.
42. Scourse JD, et al. (2009) Growth, dynamics and deglaciation of the last British–Irish ice sheet: The deep-sea ice-rafted detritus record. *Quat Sci Rev* 28:3066–3084.
43. Deplazes G, et al. (2013) Links between tropical rainfall and North Atlantic climate during the last glacial period. *Nat Geosci* 6:213–217.
44. Henry LG, et al. (2016) North Atlantic ocean circulation and abrupt climate change during the last glaciation. *Science* 353:470–474.
45. Wohlfarth B, et al. (2008) Rapid ecosystem response to abrupt climate changes during the last glacial period in western Europe, 40–16 ka. *Geology* 36:407–410.
46. Sirocko F, et al. (2016) The ELSA-Vegetation-Stack: Reconstruction of Landscape Evolution Zones (LEZ) from laminated Eifel maar sediments of the last 60,000 years. *Global Planet Change* 142:108–135.
47. An Z, et al. (2012) Interplay between the Westerlies and Asian monsoon recorded in Lake Qinghai sediments since 32 ka. *Sci Rep* 2:619.
48. Haesaerts P, et al. (2010) Charcoal and wood remains for radiocarbon dating Upper Pleistocene loess sequences in Eastern Europe and Central Siberia. *Palaeogeogr Palaeoclimatol Palaeoecol* 291:106–127.
49. Nigst PR, et al. (2014) Early modern human settlement of Europe north of the Alps occurred 43,500 years ago in a cold steppe-type environment. *Proc Natl Acad Sci USA* 111:14394–14399.
50. Hatté C, Pessenda L-C, Lang A, Paterne M (2001) Development of accurate and reliable ^{14}C chronologies for loess deposits: Application to the loess sequence of Nussloch (Rhine valley, Germany). *Radiocarbon* 43:611–618.
51. Hatté C, Morvan J, Noury C, Paterne M (2001) Is classical Acid-Alkali-Acid treatment responsible for contamination? An alternative proposition. *Radiocarbon* 43:177–182.
52. Lang A, et al. (2003) High-resolution chronologies for loess: Comparing AMS ^{14}C and optical dating results. *Quat Sci Rev* 22:953–959.
53. Bibus E, Frechen M, Kösel M, Rähle W (2007) Das jungpleistozäne Lößprofil von Nußloch (SW-Wand) im Aufschluss der Heidelberger Zement AG. *Esizeitalt Gegenw* 56:227–255.
54. Tissoux H, et al. (2010) OSL and ESR studies of Aeolian quartz from the Upper Pleistocene loess sequence of Nussloch (Germany). *Quat Geochronol* 5:131–136.
55. Gocke M, et al. (2014) Introducing an improved multi-proxy approach for paleoenvironmental reconstruction of loess–paleosol archives applied on the Late Pleistocene Nussloch sequence (SW Germany). *Palaeogeogr Palaeoclimatol Palaeoecol* 410:300–315.
56. Zöller L, Stremme H, Wagner GA (1988) Thermolumineszenz-datierung an Löss-Paläoboden-Sequenzen von Nieder-, Mittel- und Oberrhein/Bundesrepublik Deutschland. *Chem Geol* 73:39–62.
57. Evin J, Maréchal J, Pachiaudi C, Puisségur J-J (1980) Conditions involved in dating terrestrial shells. *Radiocarbon* 22:545–555.
58. Frechen M, Terhorst B, Rähle W (2007) The Upper Pleistocene loess/palaeosol sequence from Schatthausen in North Baden-Württemberg. *Eiszeitalt Gegenw* 56:212–227.
59. Schirmer W (2012) Rhine loess at Schwalbenberg II – MIS 4 and 3. *E&G Quat Sci J* 61:32–47.
60. Goodfriend GA, Stipp JJ (1983) Limestone and the problem of radiocarbon dating of land-snail shell carbonate. *Geology* 11:575–577.
61. Pigati JS, Rech JA, Nekola JC (2010) Radiocarbon dating of small terrestrial gastropod shells in North America. *Quat Geochronol* 5:519–532.
62. Pustovoytov K, Terhorst B (2004) An isotopic study of late Quaternary loess-paleosol sequence in SW Germany. *Rev Mex Cienc Geol* 21:88–93.
63. Canti M (1998) Origin of calcium carbonate granules found in buried soils and Quaternary deposits. *Boreas* 27:275–288.
64. Hodson ME, et al. (2015) Biomineralisation by earthworms - an investigation into the stability and distribution of amorphous calcium carbonate. *Geochem Trans* 16:4.
65. Antoine P (2012) Données stratigraphiques et sédimentologiques. *Quaternaire* 5:13–19.
66. Canti M, Bronk-Ramsey C, Hua Q, Marshall P (2015) Chronometry of pedogenic and stratigraphic events from calcite produced by earthworms. *Quat Geochronol* 28:96–102.
67. Tisnérat-Laborde N, Poupeau J-J, Tannau J-F, Paterne M (2001) Development of a semi-automated system for routine preparation of carbonate samples. *Radiocarbon* 43:299–304.
68. Cottereau E, et al. (2007) Artemis, the new ^{14}C AMS at LMC14 in Saclay, France. *Radiocarbon* 49:291–299.
69. Czernik J, Goslar T (2001) Preparation of graphite targets in the Gliwice Radiocarbon Laboratory for AMS ^{14}C dating. *Radiocarbon* 43:283–291.
70. Goslar T, Czernik J, Goslar E (2004) Low-energy 14C AMS in Poznan Radiocarbon Laboratory, Poland. *Nucl Instrum Methods Phys Res B* 223-224:5–11.
71. Reimer PJ, et al. (2013) IntCal13 and Marine13 radiocarbon age calibration curves 0–50,000 years cal BP. *Radiocarbon* 55:1869–1887.

Supporting Information

Moine et al. 10.1073/pnas.1614751114

SI Text

Simplified description of the units of the Nussloch loess series and chronoclimatic attributions.

S: Prequaternary substratum

Saalian:

1: Calcareous loess

Eemian:

2a and 2b: Truncated textural B horizon of brown leached soil

Weichselian early glacial:

3 and 4: Gray forest soil on colluvium

5: Humic steppe soil

Weichselian lower pleniglacial:

6–12: Laminated sandy–loamy colluvium and calcareous and sandy loess

Weichselian middle pleniglacial:

13: Aeolian sands

P4-2 [LGS (Lower Gräselberger Soil)], 14 [UGS (Upper Gräselberger Soil)], and 20 [LS (Lohne Soil)]: Boreal brown soil horizons (weathered B horizons of cambisols)

P4-2a, 16, and 18: Tundra gleys/gelic gleysols (Gm1–Gm3)

17 and 19: Homogeneous calcareous loess

Weichselian upper pleniglacial:

21b, 22, 23b, 24a, 25, 27, 30b, 31, 33b, 38a, 38c, and 38e: Homogeneous loess

36 and 37b: Weakly laminated loess

24b, 29, 32, and 34: Laminated loess with cryodessication microcracks

21a, 21c, 23a, 23c, 23d, 26, 28, and 35: Main tundra gley horizons (G1–G4 and G7)

30a, 30c, 33a, 30c, 37a, 30c, 38b, and 30d: Incipient tundra gleys

Holocene:

39: Surface soil

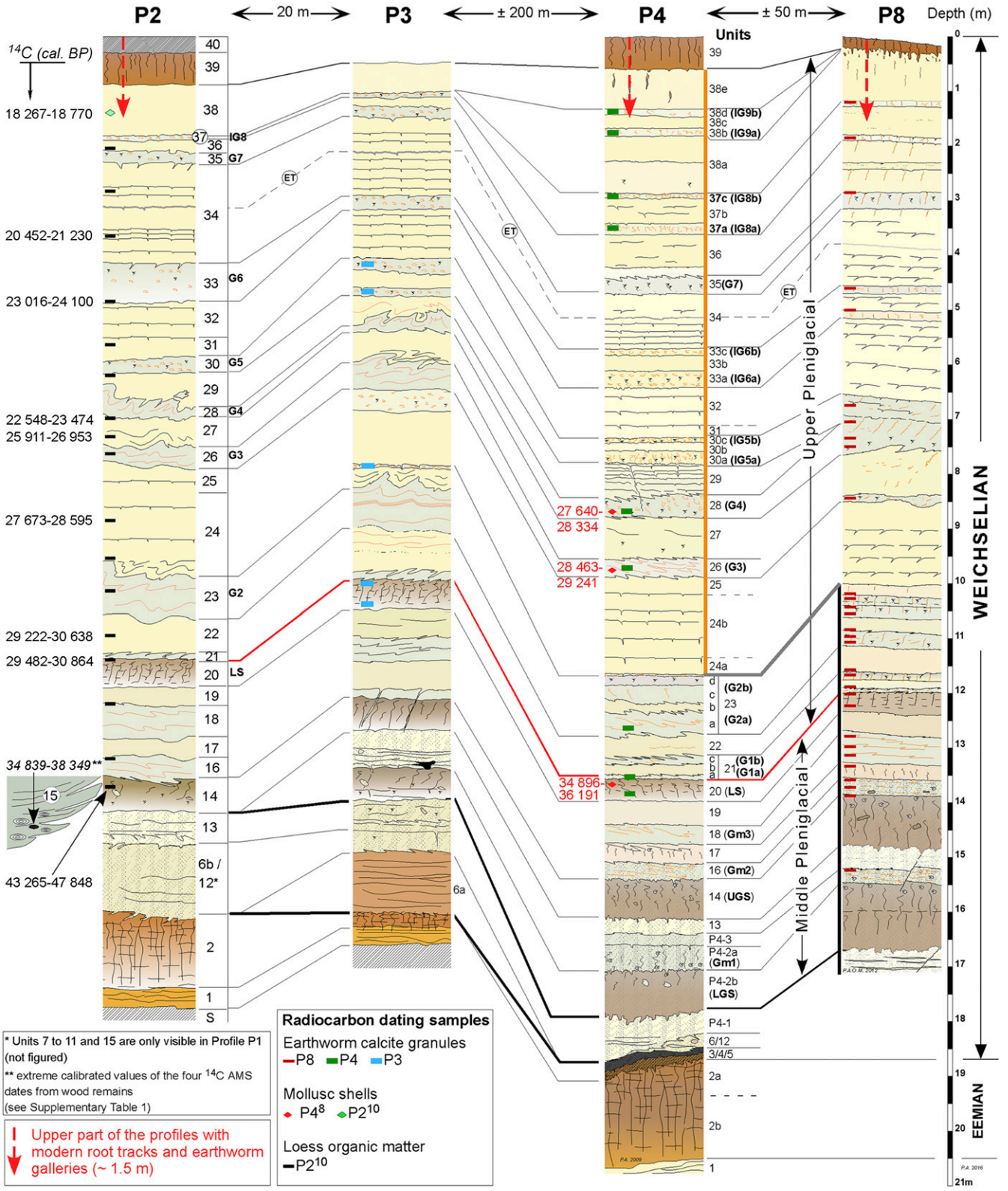

Fig. S1. Location of the dated samples throughout Nussloch P3, P4, and P8 profiles. Detailed stratigraphical descriptions and correlations are extensively described in previous publications (14, 23), except for the P8 profile. Most reliable radiocarbon ages on loess organic matter (50) are displayed along P2 profile as well as several others obtained on mollusk shells along P2 (50) and P4 (53). A summarized description of all sedimentary units is provided in *SI Text*. ET, Eltville tephra; LGS, Lower Gräselberg Soil; LS, Lohne Soil; UGS, Upper Gräselberg Soil.

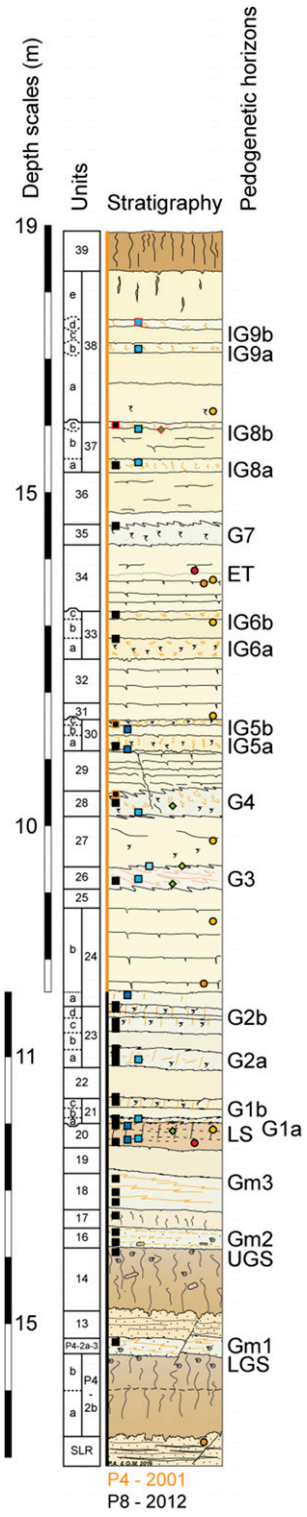

Fig. S2. Units numbering throughout the Nussloch P4–P8 composite loess profile. ET, Eltville tephra; LGS, Lower Gräselberg Soil; LS, Lohne Soil; UGS, Upper Gräselberg Soil.

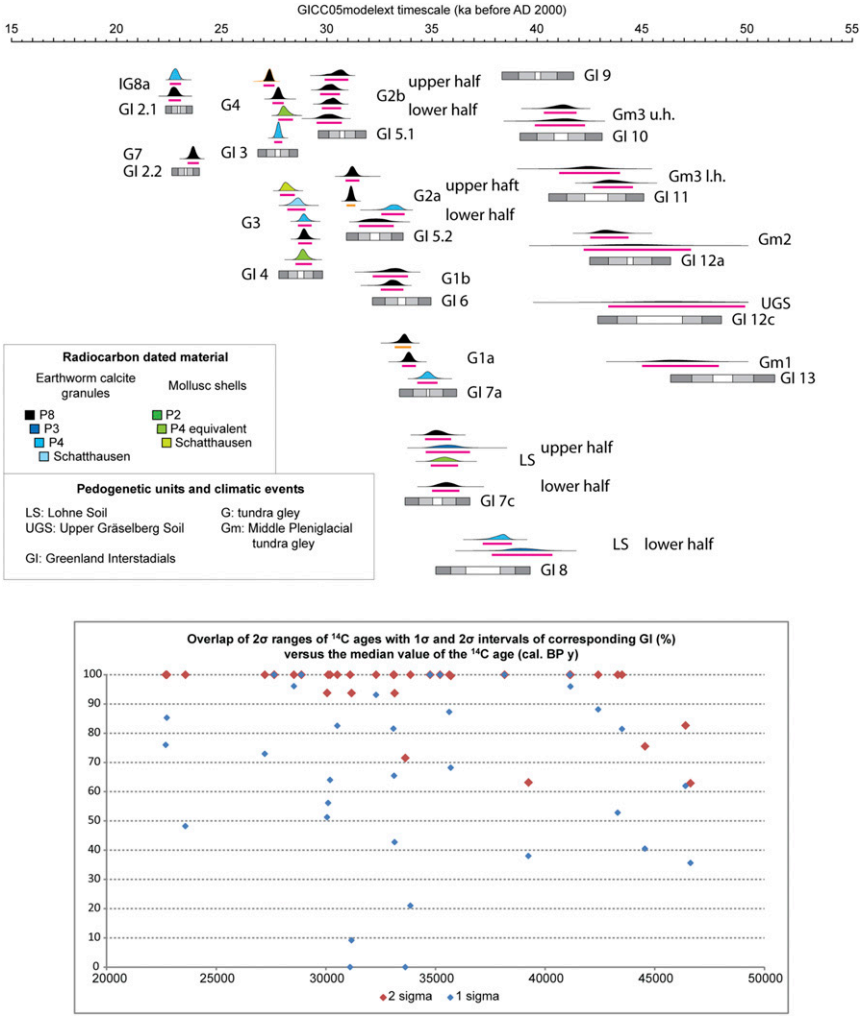

Fig. S3. Comparison of earthworm granule radiocarbon ages from tundra gleys and arctic to boreal brown soils with time intervals of corresponding Greenland interstadials (GIs). ^{14}C ages have been calibrated in thousand years before year 2000 (before AD 2000). The one-half and full values of the maximum counting errors (MCE) of the GICC05modelext age model (24) have been subtracted for onset and added for offsets to calculate GI intervals at 1σ (light gray) and 2σ (dark gray), respectively, on the basis of basic GI time interval (white). Orange bars highlight 2σ ranges of ^{14}C ages that match only with the 2σ range of their corresponding GI interval. LS, Lohne Soil.

Table S1. Radiocarbon ages of earthworm calcite granule samples from breeding experiments and the Nussloch loess–paleosoils sequence and additional radiocarbon and luminescence ages from this site represented on Fig. 2

Sample name/unit number (pedogenetic horizon)	Laboratory code	Material	Conventional age	Calibrated age: IntCal13-2s		Source
				Minimum–maximum (probability)	Median	
Compost organic matter	SacA 38251	Organic matter	270 ± 30	[1–2] (0.001)	319	This study
Compost organic matter	SacA 38251	Organic matter	270 ± 30	[153–168] (0.06)		
Compost organic matter	SacA 38251	Organic matter	270 ± 30	[282–333] (0.493)		
Compost organic matter	SacA 38251	Organic matter	270 ± 30	[353–435] (0.446)		
$CaCO_3$	SacA 35801	$CaCO_3$ powder	48,330 ± 2,370	—	—	This study
Breeding without $CaCO_3$	SacA 35798	Earthw. Calc. Gr.	Modern	—	—	This study
Breeding with $CaCO_3$	SacA 35799	Earthw. Calc. Gr.	Modern	—	—	This study
P8 120–125/37c (IG8b)	SacA 33525	Earthw. Calc. Gr.	15,460 ± 50	[18,592–18,833] (1.00)	18,726	This study
P8 185–190/37c (IG8a)	SacA35802	Earthw. Calc. Gr.	18,830 ± 130	[22,423–23,006] (1.00)	22,697	This study
P8 285–290/35 (G7)	SacA 33526	Earthw. Calc. Gr.	19,580 ± 70	[23,331–23,864] (1.00)	23,593	This study
P8 460–465/33c (IG6b)	SacA 33529	Earthw. Calc. Gr.	20,240 ± 80	[24,062–24,540] (1.00)	24,311	This study
P8 500–505/33a (IG6a)	SacA 35803	Earthw. Calc. Gr.	20,960 ± 100	[25,027–25,586] (1.00)	25,313	This study
P8 675–680/30a–b (cpx IG5)	SacA 33527	Earthw. Calc. Gr.	21,480 ± 90	[25,605–25,970] (1.00)	25,793	This study
P8 705–710/30a–b (cpx IG5)	SacA 35804	Earthw. Calc. Gr.	22,250 ± 120	[26,126–26,928] (1.00)	26,476	This study
P8 735–740/28 (G4)	SacA 33530	Earthw. Calc. Gr.	22,840 ± 100	[26,938–27,459] (1.00)	27,213	This study
P8 750–755/28 (G4)	Poz–73516	Earthw. Calc. Gr.	23,470 ± 180	[27,366–27,896] (1.00)	27,637	This study
P8 845–850/26 (G3)	SacA 33528	Earthw. Calc. Gr.	24,860 ± 120	[28,591–29,236] (1.00)	28,883	This study
P8 1020–1025/23d (G2b)	Poz–73518	Earthw. Calc. Gr.	26,250 ± 240	[29,851–30,968] (1.00)	30,519	This study
P8 1025–1030/23d (G2b)	SacA 33520	Earthw. Calc. Gr.	25,870 ± 130	[29,634–30,573] (1.00)	30,103	This study
P8 1045–1050/23c (G2b)	SacA 33521	Earthw. Calc. Gr.	25,930 ± 120	[29,721–30,624] (1.00)	30,189	This study
P8 1055–1060/23c (G2b)	Poz–73511	Earthw. Calc. Gr.	25,830 ± 220	[29,468–30,654] (1.00)	30,052	This study
P8 1085–1090/23a (G2a)	Poz–73514	Earthw. Calc. Gr.	27,220 ± 260	[30,842–31,496] (1.00)	31,167	This study
P8 1095–1110/23a (G2a)	SacA 33522	Earthw. Calc. Gr.	27,100 ± 140	[30,890–31,302] (1.00)	31,102	This study
P8 1105–1110/23a (G2a)	Poz–73536	Earthw. Calc. Gr.	28,370 ± 290	[31,479–33,130] (1.00)	32,287	This study
P8 1160–1165/21c (G1b)	Poz–73515	Earthw. Calc. Gr.	28,960 ± 310	[32,137–33,807] (1.00)	33,111	This study
P8 1165–1170/21c (G1b)	SacA 33523	Earthw. Calc. Gr.	28,880 ± 180	[32,516–33,589] (1.00)	33,078	This study
P8 1190–1195–1/21a (G1a)	SacA 33532	Earthw. Calc. Gr.	29,400 ± 180	[33,183–33,960] (1.00)	33,621	This study
P8 1190–1195–2/21a (G1a)	SacA 33524	Earthw. Calc. Gr.	29,710 ± 190	[33,532–34,184] (1.00)	33,854	This study
P8 1200–1205/20 (LS)	SacA 35805	Earthw. Calc. Gr.	31,310 ± 300	[34,627–35,861] (1.00)	35,205	This study
P8 1225–1230/20 (LS)	SacA 35806	Earthw. Calc. Gr.	31,740 ± 310	[34,959–36,256] (1.00)	35,626	This study
P8 1280–1285–1/18 (Gm3)	SacA 33531	Earthw. Calc. Gr.	36,510 ± 400	[40,281–41,831] (1.00)	41,116	This study
P8 1280–1285–2/18 (Gm3)	SacA 33516	Earthw. Calc. Gr.	36,630 ± 670	[39,847–42,228] (1.00)	41,149	This study
P8 1300–1305/18 (Gm3)	Poz–73535	Earthw. Calc. Gr.	38,300 ± 900	[41,006–43,892] (1.00)	42,414	This study
P8 1315–1320/18 (Gm3)	SacA 33517	Earthw. Calc. Gr.	39,800 ± 580	[42,611–44,511] (1.00)	43,501	This study
P8 1335–1340/17	Poz–73525	Earthw. Calc. Gr.	41,500 ± 1,500	[42,511–47,838] (1.00)	44,977	This study
P8 1360–1365/16 (Gm2)	SacA 33518	Earthw. Calc. Gr.	39,560 ± 560	[42,480–44,303] (1.00)	43,305	This study
P8 1375–1380/16 (Gm2)	Poz–73528	Earthw. Calc. Gr.	41000 ± 1,500	[42,171–47,269] (1.00)	44,550	This study
P8 1390–1395/15 (UGS)	Poz–73529	Earthw. Calc. Gr.	43,000 ± 2,000	[43,339–49,849] (1.00)	46,395	This study
P8 1525–1530/P4–2a–3 (Gm1)	SacA 33519	Earthw. Calc. Gr.	43,340 ± 890	[44,949–48,595] (1.00)	46,623	This study
P3 1190–1200/30c (IG5b)	Poz–73532	Earthw. Calc. Gr.	22,300 ± 170	[26,124–27,068] (1.00)	26,561	This study
P3 1140–1150/30a (IG5a)	Poz–73534	Earthw. Calc. Gr.	22,470 ± 160	[26,320–27,213] (1.00)	26,782	This study
P3 810–820/24	Poz–73526	Earthw. Calc. Gr.	25,050 ± 290	[28,473–29,794] (1.00)	29,107	This study
P3 600–610/20 (LS)	Poz–73530	Earthw. Calc. Gr.	31,800 ± 500	[34,659–36,759] (1.00)	35,692	This study
P3 570–580/20 (LS)	Poz–73531	Earthw. Calc. Gr.	34,700 ± 600	[37,802–40,677] (1.00)	39,234	This study
P4 1750–1760/38d (IG9b)	SacA 46572	Earthw. Calc. Gr.	12,200 ± 70	[13,814–14,353] (1.00)	14,092	This study
P4 1710–1720/38b (IG9a)	SacA 46571	Earthw. Calc. Gr.	17,470 ± 110	[20,766–21,456] (1.00)	21,102	This study
P4 1590–1600/37c (IG8b)	SacA 46570	Earthw. Calc. Gr.	18,400 ± 100	[21,961–22,476] (1.00)	22,274	This study
P4 1540–1550/37a (IG8a)	SacA 46569	Earthw. Calc. Gr.	18,890 ± 100	[22,485–23,015] (1.00)	22,748	This study
P4 1010–1020/28 (G4)	SacA 20771	Earthw. Calc.Gr.	23,480 ± 110	[27,447–27,828] (1.00)	27,645	This study
P4 910–920/26 (G3)	SacA 20770	Earthw. Calc. Gr.	24,850 ± 120	[28,581–29,222] (1.00)	28,874	This study
P4 620–630/23d (G2a)	SacA 20706	Earthw. Calc. Gr.	28,930 ± 200	[32,541–33,652] (1.00)	33,132	This study
P4 540–550/21 (G1a)	SacA 20705	Earthw. Calc. Gr.	30,830 ± 230	[34,258–35,212] (1.00)	34,747	This study
P4 510–520/20 (LS)	SacA 20704	Earthw. Calc. Gr.	33,750 ± 230	[37,021–38,866] (1.00)	38,143	This study
Schatthausen/SH9 (G3)	UtC10628	Earthw. Calc. Gr.	24,510 ± 190	[28,072–28,939] (1.00)	28,542	Refs. 58 and 62
P2/37c	Gif A–96221	Mollusk shell	15,260 ± 110	[18,267–18,770] (1.00)	18,525	Ref. 50
P4 equivalent/28 (G4)	KIA 12346	Mollusk shell	23,870 ± 170	[27,640–28,334] (1.00)	27,932	Ref. 52
P4 equivalent/26 (G3)	KIA 12347	Mollusk shell	24,790 ± 160	[28,463–29,241] (1.00)	28,825	Ref. 52
P4 equivalent/20 (LS)	KIA 12348	Mollusk shell	31,660 ± 310	[34,896–36,191] (1.00)	35,544	Ref. 52
Schatthausen/SH9 (G3)	UtC10626	Mollusk shell	23,990 ± 160	[27,725–28,426] (1.00)	28,036	Refs. 58 and 62

Table S1. Cont.

Sample name/unit number (pedogenetic horizon)	Laboratory code	Material	Conventional age	Calibrated age: IntCal13-2s		Source
				Minimum–maximum (probability)	Median	
P2 285/34	NU–1	TL polymineral	22,100 ± ?	—	—	Ref. 56
P2 730/20	NU–7	TL polymineral	34,800 ± 3,700	—	—	Ref. 56
P4 524/34	NUP4–0809	OSL quartz	23,100 ± 1,900	—	—	Ref. 53
P4 1131/24b	NUP4–0806	OSL quartz	29,500 ± 2,100	—	—	Ref. 53
P4 1808/SLR	NUP4–0801	OSL quartz	54,200 ± 4,100	—	—	Ref. 53
P2011 125/38a	BT1135	OSL quartz	17,600 ± 1,700	—	—	Ref. 55
P2011 290/34	BT1016	OSL quartz	27,500 ± 1,800	—	—	Ref. 55
P2011 360/33b	BT1178	OSL quartz	23,500 ± 2,300	—	—	Ref. 55
P2011 485/31	BT1018	OSL quartz	29,400 ± 1,700	—	—	Ref. 55
P2011 540/27	BT1180	OSL quartz	31,100 ± 2,900	—	—	Ref. 55
P2011 645/24b	BT1020	OSL quartz	34,900 ± 2,200	—	—	Ref. 55
P2011 995/20	BT1022	OSL quartz	35,100 ± 2,300	—	—	Ref. 55

Breeding experiment samples are of modern age, and conventional ages cannot be calculated. Their F14C values of 1.0250 ± 0.0037 (without $CaCO_3$) and 1.0245 ± 0.0038 (with $CaCO_3$) support their modern age. Earthw. Calc. Gr., earthworm calcite granules; LS, Lohne Soil; TL, thermoluminescence; UGS, Upper Gräselberg Soil.

Table S2. Successive correlation frames of Nussloch soil horizons with GIs

	P2 (23)		P2 (18)		P4 (16)		P3 (17)		P4 (14)			P4 equivalent (19)		P8–P4 synthesis (this study)						
Chronostratigraphy	Pedogenetic horizons	GIs	Pedogenetic horizons	GIs	Pedogenetic horizons	GIs	Pedogenetic horizons	GIs	Unit labels	Pedogenetic horizons	GIs	Pedogenetic horizons	GIs	Profiles	Unit labels	Pedogenetic horizons	ECG-based ^{14}C time intervals (cal. B.P. y)	GIs	NorthGRIP GI time intervals taking into account MCE (cal. b2k y)	Greenland [Ca^{2+}] minimums (cal. b2k y)
Weichselian Upper Pleniglacial part of the Nussloch loess sequence																				
	—		—		IG9b		—		38c	IG9b		—			38d	IG9b	13,814–14,353*		—	~20,200
	—		—		IG9a		—		38b	IG9a		—			38b	IG9a	20,766–21,456		—	~20,700
	—		G8 cpx	GI 2.1	IG8b	GI 2.1	G8 cpx	GI 2.1	37c	IG8b		—			37c	IG8b	18,592–18,833* 21,961–22,476		—	~21,900
	—				IG8a				37a	IG8a		—			37a	IG8a	22,485–23,015 22,423–23,006	GI 2.1	22,327–23,603	
	—		G7	GI 2.2	G7	GI 2.2	G7	GI 2.2	35	G7	GI 2.2–2.1	—			35	G7	23,331–23,864	GI 2.2	22,630–23,936	
	—		G6 cpx		IG6b		G6 cpx		33c	IG6b		—			33c	IG6b	24,062–24,540		—	~24,600
	—				IG6a				33a	IG6a		—		P4	33a	IG6a	25,027–25,586		—	~25,000
	—		G5 cpx		IG5b		G5b		30b	IG5b		—			30c	IG5b	25,605–25,970 26,124–27,068		—	~26,200
	—				IG5a		G5a		30a	IG5a		—			30a	IG5a	26,126–26,928 26,320–27,213		—	~27,200
	—		G4	GI 3	G4	GI 3	G4	GI 3	28	G4	GI 3	—			28	G4	26,938–27,459 27,366–27,896 27,447–27,828	GI 3	26,718–28,612	
	—		G3	GI 4	G3	GI 4	G3	GI 4	26	G3	GI 4	—			26	G3	28,072–28,939 28,581–29,222 28,591–29,236	GI 4	27,713–29,798	
	—		—		—		24 (Base)	GI 5	23a	G2b		—			23d	G2b	29,851–30,968 29,634–30,573	GI 5.1	29,592–31,864	
	—		G2 cpx	GI 5	G2b	GI 5	G2 cpx	GI 6	23b		GI 5	—			23c		29,721–30,624 29,468–30,654			
	—				G2a	GI 6			23d	G2a	GI 6	—		P8	23a	G2a	30,842–31,496 30,890–31,302 32,541–33,652 31,479–33,130	GI 5.2	30,933–33,632	
	—		G1 cpx	GI 6	G1 cpx	GI 7	G1 cpx	GI 7	21a	G1b		—			21c	G1b	32,137–33,807 32,516–33,589	GI 6	32,169–34,952	
	—								21c	G1a		—			21a	G1a	3,3183–33,960 34,258–35,212 33,532–34,184	GI 7a	33,454–36,173	
Weichselian Middle Pleniglacial part of the Nussloch loess sequence																				
	Lohne Soil	GI 8 (+ GI 7–6?)	—		Lohne Soil	GI 8	—		20	Lohne Soil	GI 7	Lohne Soil	GI 7–6–5		20	Lohne Soil	34,627–35,861 34,659–36,759 34,959–36,256	GI 7c	33,721–36,801	
																	37,021–38,866 37,802–40,677	GI 8	35,183–38,268	
	TK	GI 9, 10, or 11	—		—		—		15	TK	GI 8	TK	GI 8		15	TK	—	—	—	
	—		—		—		—		—	—		—			18	Gm3	40,281–41,831 39,847–42,228	GI 10	39,185–43,093	
														P8			41,006–43,892 42,611–44,511	GI 11	40,558–45,076	
	—		—		—		—		—	—		—			16	Gm2	42,480–44,303 42,171–47,269	GI 12a	42,500–46,351	
	Upper Gräselberg Soil	GI 12 (+ GI 14?)	—		—		—		—	—		—			14	Upper GS	43,339–49,849	GI 12c	42,884–48,772	
	—		—		—		—		—	—		—			P4–2a–3	Gm1	44,949–48,595	GI 13	46,352–51,311	
	—		—		—		—		—	—		—			P4–2b–b	Lower GS	—	GI 14a	47,549–53,636	
	—		—		—		—		—	—		—			P4–2b–a		—	GI 14c	49,516–56,249	

Maximum counting errors (MCEs) (24) added and deduced from older and lower age boundaries are given. b2k, before AD 2000; cpx, complex; ECG, earthworm calcite granule; TK, Thermokarst.
*Discarded rejuvenated ages (*Methods*).